J. Fluid Mech. (1975), *vol.* 71, *part* 1, *pp.* 15–42
Printed in Great Britain

Pulsatile flow in curved pipes

By F. T. SMITH
Mathematics Department, Imperial College, London

(Received 17 October 1974)

The characteristics of some flows that occur when fluid is driven through a curved tube are disclosed for an imposed pressure gradient of pulsatile nature, varying sinusoidally with time about a non-zero mean. The fully developed motion depends on three parameters, a traditional Dean number D, a frequency-related parameter β and a secondary Reynolds number R_s, it being assumed that the pipe's radius of curvature is much greater than its cross-sectional dimensions. The theoretical description of the flow field is extended from the steady and purely oscillatory limits hitherto studied to all the key situations arising when R_s is of order unity and one of the other parameters β or D takes a large or small value. During this analysis, which in certain cases involves the interactions between steady boundary layers and Stokes layers, a number of pulsatile motions are revealed and the manner in which at high frequencies the secondary motion can change its direction, from inward 'centrifuging' to outward, is also explained. Two further illustrations of pulsating motions, stemming from the steady limit, produce an alternative mode of transition from steady boundary-layer flow to the boundary-layer flows occurring when $R_s \sim 1$. The study, which mainly deals with the flow in an arbitrary cross-section, lays down a formal basis for deriving the fundamental attributes of many physical situations, some of which are expressible in terms of crucial modifications to, or combinations of, flow problems whose properties are already appreciated.

1. Introduction

However remote from the particular real pipe-flow situations of concern to physiologists and engineers, the determination of the characteristics of fluid flow down a perfectly smooth pipe of uniform cross-section and coiled in a circle is nevertheless a good starting point for a theoretical description. The considerable nonlinear effects directly attributable to the curvature are then taken into account, and from the physiological standpoint, leaving aside the influences of tube branchings and non-uniformity of cross-section, among others, the interactions produced when a time-dependent pressure gradient acts along the pipe can be expected to provide greater insight into the fluid dynamics operative in (for example) aortic blood flow.

Two fundamental theoretical approaches have so far been made towards evaluation of the fully developed flow in a tube whose radius of curvature R is much greater than its typical cross-sectional dimension a ($= \delta R$). The first,

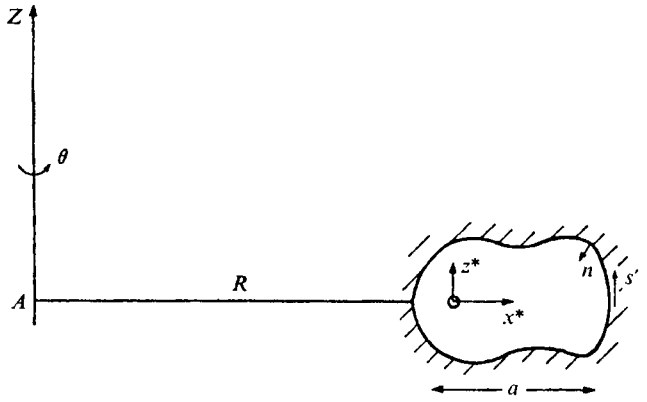

FIGURE 1. Cross-section of the tube and the co-ordinate system.

dealing with the actions of a steady pressure gradient, originated with Dean's (1927, 1928) papers, and a review of the main work on steady pipe flows is given in a related paper (Smith 1975). The second approach, which is discussed in § 3 below, is due to Lyne (1971), who assessed the motion induced in a circular tube by a pressure gradient that varies sinusoidally with time t about a zero mean.

In the current study we consider a number of the unsteady laminar flow features arising when a pulsatile pressure variation

$$\partial p^*/\partial(R\theta) = -[\rho^*\omega\overline{W}\cos\omega t + G] \tag{1.1}$$

is imposed along a pipe of arbitrary, but symmetric, cross-section. Here p^*, ρ^* and $\overline{W}$ are respectively the pressure, density and a characteristic velocity of the contained fluid, which is incompressible and of kinematic viscosity ν, while ω denotes the frequency and G the constant steady component of the pulsating pressure gradient. θ measures the angular displacement around the axis AZ, and local co-ordinates (x^*, z^*) in the pipe cross-section will subsequently be used, as shown in figure 1. Clearly the properties of the fluid motion will depend largely on the fluid itself and on the size of G in relation to the frequency and amplitude of the oscillatory component in (1.1); for instance, a delicate interplay between the inward centrifuging predicted (and realized experimentally) by Lyne (1971) and the outward streaming revealed by Smith (1975) can be anticipated for certain values of the governing parameters (1.7) of the motion. Our plan in this paper is to investigate some of the series of flow fields that occur in the regimes intermediate between the general oscillatory and steady cases, and the discussions will usually be relevant to any symmetric cross-section. One reason for keeping the study broadly based in this way, apart from the advantage of retaining generality, is the manner in which the choice of a triangular cross-section may lead to a similarity solution for $D \gg 1$ in the steady situation (§ 2.2), while the choice of a circular one can facilitate the analysis of oscillatory motions (§ 3) and of steady motions for small values of D (§ 2.1). The tube profile is supposed to be symmetric, however, so that only the flow in the upper half of the tube need be considered.

The equations of motion. For small values of δ the fluid motion is assumed to be directed primarily down the pipe, with secondary streaming of relative order $\delta^{\frac{1}{2}}$ taking place in the plane of the cross-section. Hence the velocity components in the directions (x^*, z^*, θ) may be written as

$$(u^*, v^*, w^*) = (\nu/a)\,(u, v, \delta^{-\frac{1}{2}}w), \tag{1.2}$$

where an asterisk indicates a dimensional variable, and generally u, v and w are of order unity. End effects in the pipe will be neglected, so the solution depends on the non-dimensional co-ordinates $(x, z) = (x^*/a, z^*/a)$ and time $\tau = \omega t$ but is independent of θ. Mass conservation is satisfied by introduction of a stream function χ such that

$$u = \partial\chi/\partial z, \quad v = -\partial\chi/\partial x, \tag{1.3}$$

working to first order in δ here and henceforth. Then the Navier–Stokes equations yield (see, for example, McConalogue & Srivastava 1968; Lyne 1971)

$$\frac{2}{\beta^2}\frac{\partial}{\partial\tau}(\nabla^2\chi) - \frac{\partial(\chi, \nabla^2\chi)}{\partial(x, z)} - 2w\frac{\partial w}{\partial z} = \nabla^4\chi, \tag{1.4}$$

$$\frac{2}{\beta^2}\frac{\partial w}{\partial\tau} - \frac{\partial(\chi, w)}{\partial(x, z)} = D + \frac{2}{\beta^3}(2R_s)^{\frac{1}{2}}\cos\tau + \nabla^2 w \tag{1.5}$$

as the governing equations with which we shall be concerned, ∇^2 standing for the Laplacian $\partial^2/\partial x^2 + \partial^2/\partial y^2$ and, as usual,

$$\frac{\partial(\alpha, \gamma)}{\partial(x, z)} \equiv \frac{\partial\alpha}{\partial x}\frac{\partial\gamma}{\partial z} - \frac{\partial\alpha}{\partial z}\frac{\partial\gamma}{\partial x}$$

for any functions $\alpha(x, z)$ and $\gamma(x, z)$. The boundary conditions to be satisfied with (1.4) and (1.5) are those of no slip:

$$\chi = \partial\chi/\partial n = w = 0 \quad \text{at the tube wall,} \tag{1.6}$$

with n denoting the direction of the inward normal to the wall (and, implicitly, symmetry about the x axis).

The parameters appearing in (1.4) and (1.5) are defined as

$$D = Ga^3\delta^{\frac{1}{2}}/\rho^*\nu^2, \quad \beta = (2\nu/\omega a^2)^{\frac{1}{2}}, \quad R_s = \delta\overline{W}^2/\omega\nu, \tag{1.7}$$

and are supposed to be $O(1)$ for the moment. The parameters (whose physical interpretations are given in Lyne 1971; McConalogue & Srivastava 1968) and the non-dimensionalization here have been selected as a compromise between those of Lyne, McConalogue & Srivastava and Smith, and direct comparison with their work is possible (see §§ 2 and 3). The other notable parameters adopted previously, $\epsilon^2 = \frac{1}{2}R_s\beta^2$ and the alternative Dean number $K = a\overline{W}\nu^{-1}\delta^{\frac{1}{2}}$, are related to those in (1.7) by

$$K = \rho^*\nu\overline{W}D/Ga^2, \quad R_s = \tfrac{1}{2}K^2\beta^2, \quad \epsilon = R_s/K, \tag{1.8}$$

while the ratio of the magnitude of the steady pressure gradient to that of the unsteady part is $G/\rho^*\omega\overline{W}$ or $2^{\frac{1}{2}}D\beta^3/4R_s^{\frac{1}{2}}$. Further, from the definition of $\overline{W}$, the down-pipe velocity is always $O(R_s^{\frac{1}{2}}\beta^{-1})$ in our parameter range.

Since for most values of β, R_s and D, (1.4) and (1.5) must be solved as they stand, which represents a formidable task, we examine below the nature of the

motion when one of the parameters D and β takes on a large or small value. The two classic limits of steady flow and purely oscillatory flow appear to be the only ones rigorously studied to date, except for the current investigation by Blenner-hassett (1976) referred to in § 4. As well as gaining some knowledge of certain aspects of pulsatile pipe flows, from consideration of limits that we regard as both important and physically sensible, we therefore aim to provide a coherent scheme accounting for the transition from completely steady to completely oscillatory motion, step by step. First the steady and oscillatory limits (cases I and II), and small perturbations from them, are discussed in §§ 2 and 3 and subsequently in §§ 4–6 we elucidate the behaviour of the solution in the intermediate limits (cases III–VIII) when R_s is $O(1)$. A complete asymptotic description is then possible. The outstanding features of these cases are the fully pulsatile motions in cases IV and VIII, the partitioning of the viscous wall layers into steady and unsteady (Stokes shear-wave) zones in cases III and IV, and the reversal in the direction of the main 'centrifuging' which happens in case III. The last two cases, IX and X in §§ 7 and 8, produce a match between cases I and IV, and are also both pulsatile, case IX being an example of a nonlinear down-pipe pulsation with unsteady secondary streaming, while the boundary layer in case X also subdivides at the interface with case IV. A brief discussion of the results is presented in § 9. Overall, the analysis constructs a formal framework from which the solution to many a physical problem may be extracted in principle, in the sense that most of the new situations explored are reducible ultimately to subtle modifications or combinations of the steady and/or unsteady limits, and these two limits are themselves fairly well understood now. Where this reduction is not possible (cases IX and X) asymptotic descriptions do serve as a guide to the general nature of the pulsatile flow.

Detailed discussion of the degeneracy that may occur near flat outside bends in certain circumstances (see Smith 1975) will be omitted here. Regarding nomenclature, since many different cases are to be assessed, our policy is to avoid the introduction of over-elaborate notation by keeping each section self-contained. All the definitions made hitherto do apply in each case, however. Lastly, the polar co-ordinates (r, ψ) associated with the Cartesians (x, z) will be used when a circular tube ($r = 1$) is under discussion.

2. The steady limit (case I)

The first study of the motion of a fluid along a curved pipe when δ is small was made by Dean (1927), who discussed some of the effects due to a uniform *steady* down-pipe pressure gradient. Dean's problem may be obtained from (1.4) and (1.5) by taking the limit $\beta \to \infty$ with $R_s \sim \beta^2$ and with D, w and χ kept fixed at order one. Supposing then that

$$\beta \gg 1, \quad R_s \beta^{-2} \sim 1, \quad D \sim 1, \tag{2.1}$$

which defines the present case I, we therefore expand the flow field asymptotically as

$$\left.\begin{aligned} w &= w_0(x,z) + \beta^{-2}(2R_s/\beta^2)^{\frac{1}{2}}\, w_1(x,z,\tau) + O(\beta^{-4}), \\ \chi &= \chi_0(x,z) + \beta^{-2}(2R_s/\beta^2)^{\frac{1}{2}}\, \chi_1(x,z,\tau) + O(\beta^{-4}). \end{aligned}\right\} \tag{2.2}$$

When substituted into the equations of motion (1.4) and (1.5), (2.2) produce at first order Dean's equations for the steady components w_0 and χ_0:

$$\left.\begin{aligned} -\partial(\chi_0, \nabla^2\chi_0)/\partial(x,z) - 2w_0\partial w_0/\partial z &= \nabla^4\chi_0, \\ -\partial(\chi_0, w_0)/\partial(x,z) &= D + \nabla^2 w_0, \end{aligned}\right\} \tag{2.3}$$

subject to $$\chi_0 = \partial\chi_0/\partial n = w_0 = 0 \quad \text{at the wall.} \tag{2.4}$$

The unsteady disturbances w_1 and χ_1 due to the small oscillatory pressure variation are given by

$$\left.\begin{aligned} -\frac{\partial(\chi_0, \nabla^2\chi_1)}{\partial(x,z)} - \frac{\partial(\chi_1, \nabla^2\chi_0)}{\partial(x,z)} - 2\frac{\partial}{\partial z}(w_0 w_1) &= \nabla^4\chi_1, \\ -\partial(\chi_0, w_1)/\partial(x,z) - \partial(\chi_1, w_0)/\partial(x,z) &= 2\cos\tau + \nabla^2 w_1. \end{aligned}\right\} \tag{2.5}$$

Here w_1 and χ_1 again satisfy the obvious no-slip wall conditions. Dean's equations (2.3) and (2.4) controlling w_0 and χ_0 have recently received a fair amount of attention; for example, for order-unity values of D accurate numerical solutions have been derived by McConalogue & Srivastava (1968) for the circle and by Cheng & Akiyama (1970) for the rectangle. Below we shall briefly consider their properties for values of $D \ll 1$ and, more especially, those discovered in the more interesting case $D \gg 1$, and simultaneously discuss the unsteady perturbations when D assumes small or large values.

2.1. $D \ll 1$

For small values of D, Dean (1927) showed that the motion reverts to a linearization about the Poiseuille flow solution for a straight pipe. Thus

$$w_0 = Dw_{00} + D^2 w_{01} + O(D^3), \quad \chi_0 = D^2\chi_{00} + D^3\chi_{01} + O(D^4), \tag{2.6}$$

which to lowest order in D leaves (2.3) in the form

$$\nabla^2 w_{00} = -1, \quad \nabla^4\chi_{00} = -2w_{00}\partial w_{00}/\partial z$$

with conditions of zero velocity at the tube wall. For instance, for a circular tube $r = 1$ the solution is (see Dean 1927)

$$w_{00} = \tfrac{1}{4}(1-r^2), \quad \chi_{00} = \tfrac{1}{1152}r(1-r^2)^2(1-\tfrac{1}{4}r^2)\sin\psi. \tag{2.7}$$

Similarly the unsteady disturbances w_1 and χ_1 can be expressed as

$$w_1 = w_{10} + Dw_{11} + O(D^2), \quad \chi_1 = D\chi_{10} + D^2\chi_{11} + O(D^3), \tag{2.8}$$

and from (2.5) we find that

$$\nabla^2 w_{10} = -2\cos\tau, \quad \nabla^4\chi_{10} = -2\partial(w_{00}w_{10})/\partial z$$

with the no-slip conditions, the relative error again being $O(D^2)$. Hence

$$w_{10} = \tfrac{1}{2}(1-r^2)\cos\tau, \quad \chi_{10} = \tfrac{1}{288}r(1-r^2)^2(1-\tfrac{1}{4}r^2)\sin\psi\cos\tau \tag{2.9}$$

for a circle. Expressions for w_{00}, χ_{00}, w_{10} and χ_{10} are also calculable for rectangular and triangular cross-sections, although they involve double series expansions.

2.2. $D \gg 1$

When D is large the steady flow is expected (initially, at least) to develop a laminar boundary-layer character, and Smith's (1975) investigation, among others, shows that this has the form of an inviscid core motion, with fluid drifting slowly outwards, supplemented by a viscous jet flow along the pipe walls in which the secondary flow is projected mainly towards the inside of the bend. In the core,

$$w_0 = D^{\frac{2}{3}} w_0^{(0)} + D^{\frac{1}{3}} w_0^{(1)} + O(1), \quad \chi_0 = D^{\frac{1}{3}} \chi_0^{(0)} + \chi_0^{(1)} + O(D^{-\frac{1}{3}}) \tag{2.10}$$

for $D \gg 1$, where

$$w_0^{(0)} = \omega_0^{(0)}(x), \quad \chi_0^{(0)} = z/w_0^{(0)\prime}(x) \tag{2.11}$$

in order to satisfy the Dean equations (2.3) to a first approximation. Here and henceforth a prime will denote differentiation with respect to the appropriate independent variable. Near the wall, $z = g(x)$ say, the boundary layer (or jet) has thickness $\sim D^{-\frac{1}{3}}$ and

$$w_0 = D^{\frac{2}{3}} W_0(s, N) + O(D^{\frac{1}{3}}), \quad \chi_0 = D^{\frac{1}{3}} X_0(s, N) + O(1), \tag{2.12}$$

where $N = D^{\frac{1}{3}} n \sim 1$, and W_0 and X_0 are found to obey

$$\left.\begin{aligned} -\frac{\partial(X_0, \partial X_0/\partial N)}{\partial(s, N)} + \frac{W_0^2 - w_0^{(0)2}}{[1+g'(x)^2]^{\frac{1}{2}}} &= \frac{\partial^3 X_0}{\partial N^3}, \\ -\partial(X_0, W_0)/\partial(s, N) &= \partial^2 W_0/\partial N^2 \end{aligned}\right\} \tag{2.13}$$

with the boundary conditions

$$\left.\begin{aligned} X_0 = \partial X_0/\partial N = W_0 = 0 \quad \text{at} \quad N = 0, \\ X_0(s, \infty) = g(x)/w_0^{(0)\prime}(x), \quad W_0(s, \infty) = w_0^{(0)}(x). \end{aligned}\right\} \tag{2.14}$$

Here s denotes distance along the tube wall, starting from the outside of the bend, and it is necessary that $g'(x)$ be finite and that a stagnation point be imposed at the inside of the bend (see Smith 1975). The reason for the orders of magnitude in (2.10) and (2.12) is that in the viscous layer the centrifugal effect has to force the secondary streaming, whereas the primary motion is dominated by the interplay between inertia and viscous forces alone, and it is in the core that the large steady pressure gradient promotes the secondary flow.

A number of other researchers, Blennerhassett (1976), Prof. N. Riley, Prof. J. T. Stuart and Ito (1969), have been aware of the large-D problem (2.13) and (2.14) for a circle, and we now know (Smith 1975) that an attached-flow solution exists in a certain simple situation, but not in another equally simple case. Specifically, Smith proves that, almost certainly, *no* attached solution exists for the rectangle, when $g(x) = d > 0$, say, but a well-defined similarity solution can be found for the triangle, when $g(x) = x \tan\alpha$ $(0 \leqslant x \leqslant 1)$. For the latter configuration

$$W_0 = B x^{\frac{5}{6}} H(\eta), \quad X_0 = (B/\cos\alpha)^{\frac{1}{2}} x^{\frac{7}{6}} F(\eta), \tag{2.15a}$$

where $\eta = (B\cos\alpha)^{\frac{1}{2}} N x^{\frac{1}{6}}$, and H and F are governed by a pair of nonlinear ordinary differential equations, with

$$F(0) = F'(0) = H(0) = F'(\infty) = H(\infty) - 1 = 0.$$

The numerical solution has the main properties

$$F''(0) = 1{\cdot}820, \quad H'(0) = 1{\cdot}119, \quad F(\infty) = 0{\cdot}562 \tag{2.15b}$$

and for consistency $B = 1{\cdot}659 \sin^{\frac{2}{3}}\alpha \cos^{-\frac{1}{3}}\alpha$. The question raised in Smith (1975) of the range of validity of (2.15a) for the triangle is not yet settled (if it applies throughout $0 < x < 1$, for example, then an inertia-driven boundary layer is set up near the outside of the bend $x = 1$), but for any cross-section that comes to a point at the inside of the bend $x = 0$, the solution, provided that it exists elsewhere, has the form (2.15) locally near $x = 0$. On the other hand, since the rectangular case has no such large-D solution, neither has any cross-section with a flat inner side.

The assumption of a solution for large values of D for any particular cross-section must accordingly be made with some caution. It is our intention in the forthcoming sections to assume implicitly that a solution does exist for the third fundamental cross-section, namely the circular one, for which (2.13) becomes

$$\left.\begin{aligned} \frac{\partial(X_0, \partial X_0/\partial\rho)}{\partial(\rho,\psi)} + (W_0^2 - w_0^{(0)2})\sin\psi &= \frac{\partial^3 X_0}{\partial\rho^3}, \\ \partial(X_0, W_0)/\partial(\rho,\psi) &= \partial^2 W_0/\partial\rho^2. \end{aligned}\right\} \tag{2.16}$$

Here $\psi = s$ measures the angle from the outside of the bend $\psi = 0$ and

$$\rho = (1-r)\,D^{\frac{1}{3}}$$

replaces N. Also,

$$w_0^{(0)} = w_0^{(0)}(\cos\psi), \quad \chi_0^{(0)} = -\frac{z\sin\psi}{dw_0^{(0)}/d\psi}. \tag{2.17}$$

To lend support to our assumption we note the following gratifying features of (2.16), subject to (2.14). First, for consistency close to the inside of the bend $\psi = \pi$, where the boundary layer finishes, it is found that the solution must develop in non-integral powers of $\theta = \pi - \psi$ because the wall becomes 'vertical', and we find that

$$w_0^{(0)} = \hat{A}\theta^{\frac{4}{3}}[1 + \hat{\kappa}\theta^2 + O(\theta^4)], \quad \chi_0^{(0)} = (3z/4\hat{A})\,\theta^{\frac{2}{3}}[1 - \tfrac{1}{6}\theta^2(1 + 15\hat{\kappa}) + O(\theta^4)] \tag{2.18a}$$

in the core, with the constants $\hat{A}$ and $\hat{\kappa}$ unknown. In the boundary layer

$$W_0 = \hat{A}\theta^{\frac{1}{3}}[\hat{H}(\hat{\eta}) + \hat{\kappa}\theta^2\hat{H}_1(\hat{\eta}) + O(\theta^4)], \quad X_0 = \hat{A}^{\frac{1}{2}}\theta^{\frac{2}{3}}[\hat{F}(\hat{\eta}) + \theta^2\hat{F}_1(\hat{\eta}) + O(\theta^4)] \tag{2.18b}$$

($\hat{\eta} = \hat{A}^{\frac{1}{2}}\rho\theta^{\frac{2}{3}}$). Substituting into (2.16) gives the nonlinear ordinary differential equations

$$\hat{F}''' = \tfrac{5}{3}\hat{F}\hat{F}'' - \tfrac{7}{3}\hat{F}'^2 + \hat{H}^2 - 1, \quad \hat{H}'' = \tfrac{5}{3}\hat{F}\hat{H}' - \tfrac{4}{3}\hat{F}'\hat{H} \tag{2.18c}$$

for $\hat{F}$ and $\hat{H}$, for which the boundary conditions are as in (2.15a) ff. The solution here, obtained numerically using Burggraf's program (see Smith 1975) and displayed in figure 2, has the principal properties

$$\hat{F}''(0) = 1{\cdot}595, \quad \hat{H}'(0) = 1{\cdot}265, \quad \hat{F}(\infty) = 0{\cdot}503.$$

Hence $\hat{A} = 1{\cdot}303$. The subsequent terms $\hat{H}_1, \hat{F}_1, \ldots$, in (2.18$b$) also satisfy ordinary differential equations, but of linear type, and can be calculated.

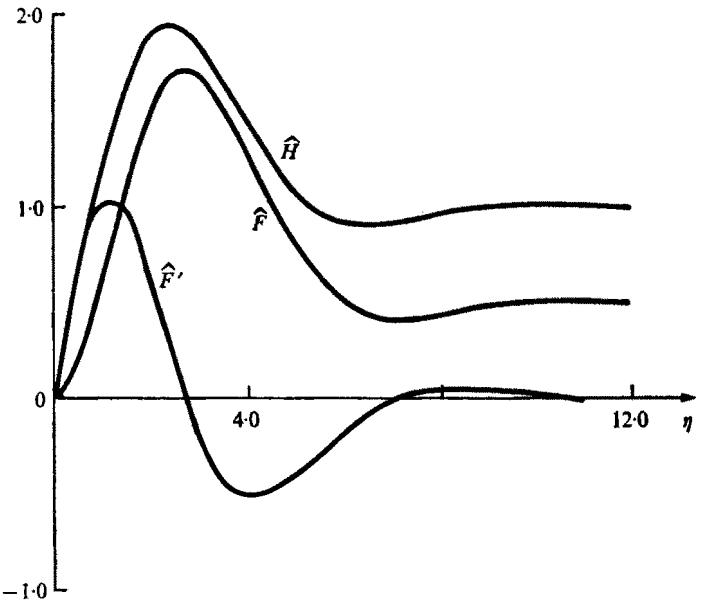

FIGURE 2. Solution curves of $\hat{F}$, $\hat{F}'$ and $\hat{H}$ *vs.* $\hat{\eta}$ for the inside of the bend in a circular tube [equations (2.18)].

The second special property associated with the circle concerns the start of the boundary layer at the outside wall $\psi = 0$, where the flow is regular. For $\psi \ll 1$ it is evident that, if $\rho_1 = \rho[w_0^{(0)}(1)]^{\frac{1}{2}}$,

$$\left.\begin{aligned} W_0 = w_0^{(0)}(1)\hat{h}(\rho_1) + O(\psi), \quad X_0 = \psi[w_0^{(0)}(1)]^{\frac{1}{2}}\hat{f}(\rho_1) + O(\psi^2), \\ w_0^{(0)}(\cos\psi) = w_0^{(0)}(1) + O(\psi), \quad \chi_0^{(0)} = \frac{\psi}{dw_0^{(0)}(1)/dx} + O(\psi^2), \end{aligned}\right\} \tag{2.19a}$$

because $\omega_0^{(0)}(1)$ being non-zero forces a non-zero initial distribution of primary flow near the wall, but the secondary streaming is initially zero by symmetry. In (2.16) this yields the following coupled equations for $\hat{h}$ and $\hat{f}$:

$$\hat{f}''' + \hat{f}\hat{f}'' - \hat{f}'^2 + 1 - \hat{h}^2 = 0, \quad \hat{h}'' + \hat{f}\hat{h}' = 0,$$

with the usual boundary conditions. The problem for $\hat{h}$ and $\hat{f}$ is identical with one solved by Stewartson (1957) and so has the properties

$$\hat{f}''(0) = 0{\cdot}953, \quad \hat{h}'(0) = 0{\cdot}463, \quad \hat{f}(\infty) = 1{\cdot}33.$$

Thence, matching the core and viscous layer,

$$dw_0^{(0)}(1)/dx = 0{\cdot}75[w_0^{(0)}(1)]^{-\frac{1}{2}}. \tag{2.19b}$$

The value of $w_0^{(0)}(1)$ must actually be fixed by the assumed solution to (2.14) and (2.16) for all ψ, but some justification that the overall solution does in truth exist comes from comparing the value of $w'(x)$ according to the above result at $x = 1$ with a typical core value predicted by McConalogue & Srivastava's (1968) computations along $\psi = 0$. Taking $2^{\frac{1}{2}}w(1) = 98{\cdot}5$ at $2^{\frac{1}{2}}D = 605{\cdot}72$ (the factors $2^{\frac{1}{2}}$ allow for the differences in definition between the last-named and the present papers), (2.19*b*) gives $w'(1) \approx 38{\cdot}4$ whereas the full numerical solution has $w'(0{\cdot}5) \doteqdot 33{\cdot}9$,

which is in fair agreement. An assessment of the accuracy of (2.18) also suggests quite a good approximation, and hence our belief in the existence of a high Dean number solution for the circle seems not unreasonable. Indeed, the very existence of the initial and terminal forms (2.19) and (2.18) is strongly supportive (cf. Belcher, Burggraf & Stewartson 1972), and the nearly completed calculations of (2.16) and (2.17) by Prof. N. Riley and Prof. S. C. R. Dennis appear to bear out our implicit assumption. However, the work undertaken below does not depend crucially on that assumption since all the ensuing results are readily modified to the triangular situation, or to any other cross-section for which a solution also exists.

Moving on now to the unsteady perturbations, we propose that when $D \gg 1$ they behave in the following manner, which is indicated by reasoning akin to that for the major flow (2.10)–(2.14). In the core,

$$w_1 = D^{-\frac{1}{3}} w_1^{(0)} + O(D^{-\frac{2}{3}}), \quad \chi_1 = D^{-\frac{2}{3}} \chi_1^{(0)} + O(D^{-1}), \tag{2.20}$$

so that

$$w_1^{(0)} = w_1^{(0)}(x, \tau), \quad \chi_1^{(0)} = z\left[\frac{2\cos\tau}{w_0^{(0)\prime}} - \frac{\partial w_1^{(0)}/\partial x}{w_0^{(0)\prime 2}}\right] \tag{2.21}$$

upon substitution into (2.5). Again the $D^{-\frac{1}{3}}$ viscous layer is required near the wall $z = g(x)$, where

$$w_1 = D^{-\frac{1}{3}} W_1(s, N, \tau) + O(D^{-\frac{2}{3}}), \quad \chi_1 = D^{-\frac{2}{3}} X_1(s, N, \tau) + O(D^{-1}). \tag{2.22}$$

Hence W_1 and X_1 satisfy

$$\left.\begin{aligned} -\frac{\partial(X_0, \partial X_1/\partial N)}{\partial(s, N)} - \frac{\partial(X_1, \partial X_0/\partial N)}{\partial(s, N)} + \frac{2[W_0 W_1 - w_0^{(0)} w_1^{(0)}]}{[1 + g'(x)^2]^{\frac{1}{2}}} &= \frac{\partial^3 X_1}{\partial N^3}, \\ -\frac{\partial(X_0, W_1)}{\partial(s, N)} - \frac{\partial(X_1, W_0)}{\partial(s, N)} &= \frac{\partial^2 W_1}{\partial N^2}, \end{aligned}\right\} \tag{2.23}$$

subject to conditions of no slip at the wall and of matching with the core at the edge of the boundary layer, i.e.

$$\left.\begin{aligned} X_1 = \partial X_1/\partial N = W_1 = 0 \quad \text{at} \quad N = 0, \\ X_1 \to g(x)\left[\frac{2\cos\tau}{w_0^{(0)\prime}} - \frac{\partial \omega_1^{(0)}/\partial x}{w_0^{(0)\prime 2}}\right], \quad W_1 \to w_1^{(0)}(x, \tau) \quad \text{as} \quad N \to \infty. \end{aligned}\right\} \tag{2.24}$$

Despite the absence of any time derivative in (2.23), the components W_1 and X_1 are nevertheless unsteady owing to the pulsatile nature of the core flow (2.21), as can be seen in (2.25) and (2.26) below.

To verify that solutions for W_1 and X_1 are possible let us consider first the features of a 'pinched' inside wall $g(x) = x\tan\alpha$ for $x \ll 1$, for which the steady motion is given in (2.15). The similarity form there motivates a search for a corresponding similarity solution to (2.23) and (2.24) and for a simple core motion. It is found that

$$w_1^{(0)} = Cx^{\frac{5}{6}}\cos\tau, \quad \text{implying} \quad \chi_1^{(0)} = \frac{6z}{5B} x^{\frac{1}{6}}\left(2 - \frac{C}{B}\right)\cos\tau, \tag{2.25}$$

while in the boundary layer

$$W_1 = Cx^{\frac{5}{6}} h(\eta)\cos\tau, \quad X_1 = C(B\cos\alpha)^{-\frac{1}{2}} x^{\frac{7}{6}} f(\eta)\cos\tau, \tag{2.26}$$

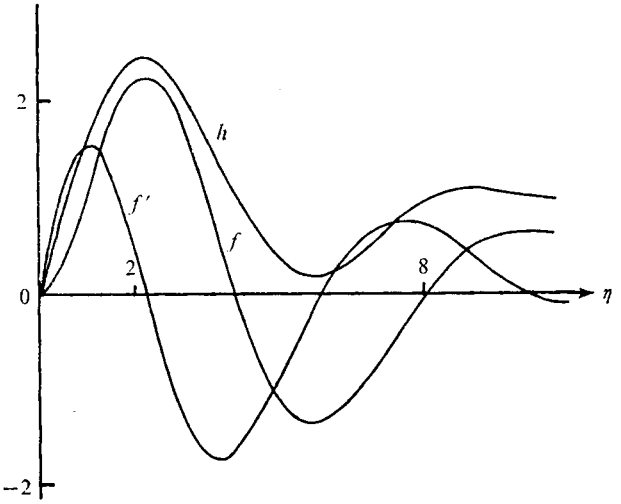

FIGURE 3. Graphs of f, f' and h *vs.* η for a pinched inside wall [equations (2.27)].

where $\eta = (B\cos\alpha)^{\frac{1}{2}}x^{\frac{1}{3}}$ and the constant factors C and $B\cos\alpha$ are introduced for convenience. Then (2.23) and (2.24) are obeyed provided that $h(\eta)$ and $f(\eta)$ satisfy

$$\left.\begin{aligned} f''' &= \tfrac{7}{6}(Ff''+fF'')-\tfrac{8}{3}F'f'+2(Hh-1), \\ h'' &= \tfrac{7}{6}(Fh'+fH')-\tfrac{5}{6}(F'h+f'H), \end{aligned}\right\} \tag{2.27}$$

with $f(0) = f'(0) = h(0) = f'(\infty) = h(\infty)-1 = 0$. Also,

$$f(\infty) = \frac{6\tan\alpha}{5B}\left(2-\frac{C}{B}\right)\frac{(B\cos\alpha)^{\frac{1}{2}}}{C}$$

then serves to determine the unknown constant C. A numerical solution of (2.27) gives

$$h'(0) = 1{\cdot}67, \quad f''(0) = 2{\cdot}51, \quad f(\infty) = 0{\cdot}63,$$

and the implied value for C is then $1{\cdot}57\sin^{\frac{2}{3}}\alpha\cos^{-\frac{1}{3}}\alpha$. Graphs of f, f' and h are drawn in figure 3.

Likewise, similarity expressions for W_1 and X_1 may be set up for the circular tube near $\psi = \pi$ and $\psi = 0$, based on the known local steady solutions (2.18) and (2.19) respectively, and it transpires that near the inside of the bend

$$\left.\begin{aligned} w_1^{(0)} = \hat{C}\theta^{\frac{4}{3}}\cos\tau, \quad \chi_1^{(0)} &= \frac{3z}{4\hat{A}}\theta^{\frac{2}{3}}\left(2-\frac{\hat{C}}{\hat{A}}\right)\cos\tau \quad \text{(core)}, \\ W_1 = \hat{C}\theta^{\frac{4}{3}}\hat{H}_1(\hat{\eta})\cos\tau, \quad X_1 &= \hat{C}\hat{A}^{-\frac{1}{2}}\theta^{\frac{5}{3}}\hat{F}_1(\hat{\eta})\cos\tau \quad \text{(boundary layer)}, \end{aligned}\right\} \tag{2.28}$$

with $\hat{F}_1$ and $\hat{H}_1$ governed by linear equations much like (2.27). The solution, obtained numerically, is given in figure 4 and has the properties

$$\hat{H}_1'(0) = 1{\cdot}99, \quad \hat{F}_1''(0) = 2{\cdot}19, \quad \hat{F}_1(\infty) = 0{\cdot}43,$$

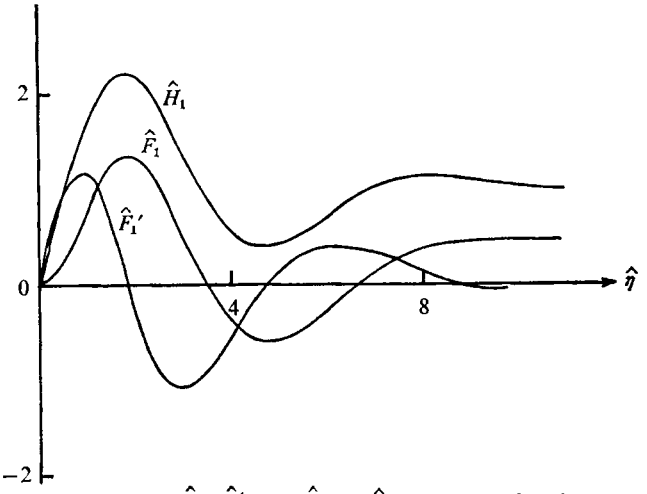

FIGURE 4. Graphs of $\hat{F}_1$, $\hat{F}_1'$ and $\hat{H}_1$ *vs.* $\hat{\eta}$ for the inside of the bend in a circular tube [equations (2.28)].

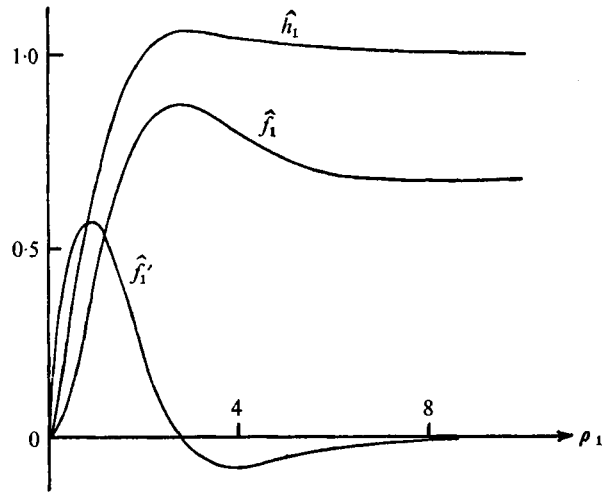

FIGURE 5. Graphs of $\hat{f}_1$, $\hat{f}_1'$ and $\hat{h}_1$ *vs.* ρ_1 for the outside of the bend in a circular tube [equations (2.29)].

so that $\hat{C} = 0{\cdot}55$. Similarly, near the outside of the bend of the circular cross-section, one finds that

$$\left.\begin{aligned} w_1^{(0)} &= \kappa_1 \cos\tau + O(\psi), \quad \chi_1^{(0)} = \psi\cos\tau\left(2-\hat{c}\left[\frac{dw_0^{(0)}}{dx}(1)\right]^{-1}\right)\Big/\frac{dw_0^{(0)}}{dx}(1) + O(\psi^2), \\ W_1 &= \kappa_1\hat{h}_1(\rho_1)\cos\tau + O(\psi), \quad X_1 = \kappa_1\psi\cos\tau\hat{f}_1(\rho_1)/\kappa^{\frac{3}{2}} + O(\psi^2), \end{aligned}\right\} \tag{2.29}$$

where $\kappa = w_0^{(0)}(1)$ and κ_1 and $\hat{c}$ are constants. Figure 5 shows the calculated solution for $\hat{f}_1, \hat{f}_1'$ and $\hat{h}_1$, which gives

$$\hat{h}_1'(0) = 0{\cdot}69, \quad \hat{f}_1''(0) = 1{\cdot}24, \quad \hat{f}_1(\infty) = 0{\cdot}66$$

and $\hat{c} = (1{\cdot}5 - 0{\cdot}37\kappa_1/\kappa^2)\kappa^{-\frac{1}{2}}$. The significance of these similarity solutions will become more apparent when case IV is examined below.

It is noted that the oscillatory perturbations in the present quasi-steady state, e.g. (2.25), are in phase with the pressure gradient and hence $\frac{1}{2}\pi$ out of phase with the majority of the pulsatile flows revealed in later sections (see §§ 3–8). The same holds for the results in § 2.1. Another point worth stressing is that in the high Dean number limit, from the definition of $\overline{W}$ in § 1,

$$K = \lambda D^{\frac{2}{3}}, \tag{2.30}$$

where λ is an order-one constant, equal to $1{\cdot}17 \sin^{\frac{2}{3}}\alpha \cos^{-\frac{1}{3}}\alpha$ for the triangle if $\overline{W}$ is defined as the average core velocity of (2.15a) (see Smith 1975). The relation (2.30) leads us to consider in §§ 7 and 8 a number of limits of the equations of motion (1.4) and (1.5) which turn out to possess interesting pulsatile characteristics. In fact the present large-D analysis matches with case IX below when (2.30) is preserved. Next, however, we shall discuss the second classic limit of the full problem (1.4) and (1.5) to have been studied: that of a purely oscillatory pressure gradient.

3. The oscillatory limit (case II)

When the Dean number D is set equal to zero in (1.5), with β and R_s kept fixed, the problem of evaluating the effects of an oscillating pressure gradient, discussed by Lyne (1971), results (although our non-dimensionalization is slightly different from his). Hence, if the solutions of his equations for R_s, $\beta \sim 1$ are written as $w_0(x,z,\tau)$ and $\chi_0(x,z,\tau)$, then for small non-zero values of D the expansions

$$w = w_0 + Dw_1 + O(D^2), \quad \chi = \chi_0 + D\chi_1 + O(D^2) \tag{3.1}$$

are appropriate. These yield the equations

$$\left.\begin{aligned} \frac{2}{\beta^2}\frac{\partial}{\partial\tau}(\nabla^2\chi_1) - \frac{\partial(\chi_0,\nabla^2\chi_1)}{\partial(x,z)} - \frac{\partial(\chi_1,\nabla^2\chi_0)}{\partial(x,z)} - 2\frac{\partial}{\partial z}(w_0 w_1) &= \nabla^4\chi_1, \\ \frac{2}{\beta^2}\frac{\partial w_1}{\partial\tau} - \frac{\partial(\chi_0,w_1)}{\partial(x,z)} - \frac{\partial(\chi_1,w_0)}{\partial(x,z)} &= 1 + \nabla^2 w_1 \end{aligned}\right\} \tag{3.2}$$

for the perturbations χ_1 and w_1 due to the presence of the small mean pressure-gradient component. The *small-D* equations (3.1) and (3.2) with the boundary conditions of no slip at the tube wall will be referred to as *case* II and in the remainder of this section various features of the flow will be considered for small and large values of β.

3.1. $\beta \ll 1$

Lyne (1971) confined his analysis of w_0 and χ_0 to the high frequency range $\beta \ll 1$. With $D \ll \beta \ll 1$ and $R_s \sim 1$ the solutions for w_1 and χ_1 are then also obtainable, as follows.

Considering first the core, where $w_0 = \beta^{-1}(2R_s)^{\frac{1}{2}}\sin\tau$, to first order $\chi_0 = \chi_0(x,z)$ is steady and governed by the two-dimensional Navier–Stokes equation (see Lyne's work)

$$-\partial(\chi_0,\nabla^2\chi_0)/\partial(x,z) = \nabla^4\chi_0 \tag{3.3}$$

under the slip conditions $\chi_0 = 0$ but $\partial\chi_0/\partial n = -\frac{1}{4}R_s\mu(x)$ at the solid surface, owing to the behaviour (3.8) below. The function $\mu(x)$ is defined for the general shape $z = g(x)$ by

$$\mu(x) = [1+g'(x)^2]^{-\frac{1}{2}}; \tag{3.4}$$

for the circle it gives a factor $\sin\psi$, while for the rectangle $\mu = 1$ on the top wall and $\mu = 0$ on the side walls. (Computed results for (3.3) with the above boundary conditions are presented by Kuwahara & Imai (1969) for the circle, with R_s ranging from zero to 2048.) w_1 and χ_1 now develop according to the formulae

$$w_1 = w_1^{(0)}(x,z)+\beta w_1^{(1)}(x,z)+O(\beta^2), \quad \chi_1 = \beta\chi_1^{(0)}(x,z,\tau)+O(\beta^2). \tag{3.5}$$

Here $w_1^{(0)}$, $w_1^{(1)}$ and $w_1^{(2)}$ are steady terms and from substitution into (3.2), $w_1^{(0)}$ and $\chi_1^{(0)}$ are controlled by the equations

$$\partial(\nabla^2\chi_1^{(0)})/\partial\tau = 2(2R_s)^{\frac{1}{2}}\sin\tau\,\partial w_1^{(0)}/\partial z, \tag{3.6}$$

$$-\partial(\chi_0, w_1^{(0)})/\partial(x,z) = 1+\nabla^2 w_1^{(0)} \tag{3.7}$$

for arbitrary values of R_s. The lower-order terms bring time dependence and viscosity into the χ and w equations respectively. We stipulate the boundary conditions

$$w_1^{(0)} = \chi_1^{(0)} = 0 \quad \text{at the pipe wall} \tag{3.8}$$

but in general $\partial\chi_1^{(0)}/\partial n$ will be non-zero there because (3.6) is inviscid. Integrating (3.6) once with respect to τ then leaves

$$\nabla^2\chi_1^{(0)} = -2(2R_s)^{\frac{1}{2}}\cos\tau\,\partial w_1^{(0)}/\partial z \tag{3.6a}$$

an arbitrary function of x, z being omitted for reasons similar to those given by Lyne (1971, § 2).

Second, in the $O(\beta)$ Stokes layer bordering the wall, w_0 remains of order β^{-1} but χ_0 is reduced to order β, the precise solutions for an arbitrary cross-section following from an extension of Lyne's work as

$$w_0 = \beta^{-1}[\sin\tau - e^{-\eta}\sin(\tau-\eta)+O(\beta)](2R_s)^{\frac{1}{2}}, \tag{3.9a}$$

$$\chi_0 = \beta\{-\tfrac{1}{4}\eta+O(1)\}R_s\mu(x)+O(\beta^2). \tag{3.9b}$$

Generally $\eta = \beta^{-1}n$, and $O(1)$ here stands for the terms in equation (3.26) of Lyne's paper that remain finite as $\eta\to\infty$. Therefore it is to be expected that in the Stokes layer

$$w_1 = \beta\eta\,T(x)+O(\beta^2), \quad \chi_1 = \beta^2 X_1+O(\beta^3), \tag{3.10}$$

where $T(x) = (\partial w_1^{(0)}/\partial x)_{n=0}$ is as yet unknown. Expansion (3.10) yields, in (3.2), the viscous balance

$$\partial^3 X_1/\partial\tau\,\partial\eta^2 = \tfrac{1}{2}\partial^4 X_1/\partial\eta^4 \tag{3.11}$$

to first order in β, other terms following readily. The constraints on (3.11) are those of no slip at $\eta = 0$ and $\partial X_1/\partial\eta \to (\partial\chi_1^{(0)}/\partial n)_{n=0} \equiv R(x)\cos\tau$ as $\eta\to\infty$, where $R(x)$, like $T(x)$, is to be ascertained from (3.6)–(3.8). Hence we deduce

$$X_1 = R(x)\{\eta\cos\tau+2^{-\frac{1}{2}}\cos(\tau+\tfrac{1}{4}\pi)+2^{-\frac{1}{2}}e^{-\eta}\sin(\tau-\eta+\tfrac{1}{4}\pi)\} \tag{3.12}$$

and the Stokes-layer solution is determined.

The remaining problem, which is to calculate $T(x)$ and $R(x)$ from (3.6)–(3.8), is in general a computational task, as is the determination of χ_0 in (3.3). It may be done analytically, however, if $R_s \ll 1$, since then $w_1^{(0)}$ is $O(1)$ and $\chi_1^{(0)}$ is $O(R_s^{\frac{1}{2}})$ whereas χ_0 is $O(R_s)$. Thus $\nabla^2 w_1^{(0)} = -1$, implying the Poiseuille flow for the circular cross-section,

$$w_1^{(0)} = \tfrac{1}{4}(1-r^2), \tag{3.13}$$

and the equation $\nabla^2 \chi_1^{(0)} = (2R_s)^{\frac{1}{2}} r \sin\psi \cos\tau$ for $\chi_1^{(0)}$, to highest order. Consequently,

$$\chi_1^{(0)} = \tfrac{1}{8}(2R_s)^{\frac{1}{2}}(r^2-1)\, r \sin\psi \cos\tau,$$

giving $R(x) = -\frac{1}{4}(2R_s)^{\frac{1}{2}} \sin\psi$ and $T(x) = \frac{1}{2}$ when R_s is small.

Again, if $R_s \gg 1$ the essential character of the solution could be anticipated by recalling Lyne's (1971) solution (5.3) for $R_s^{-1}\chi_0$, within a circle, and treating the core as an inviscid interior with viscous layers astride the Stokes layer and the centre-line. This flow is in effect encountered in a study undertaken by Blenner-hassett (1976), which is mentioned briefly in § 4.

3.2. $\beta \gg 1$

If now $R_s \sim 1$ but $\beta \gg 1$ (low frequencies), so that the motion is in a sense slow, inspection of the basic equations indicates the expansions

$$w_0 = \beta^{-3} w_{00} + O(\beta^{-6}), \quad \chi_0 = \beta^{-6}\chi_{00} + O(\beta^{-9}). \tag{3.14}$$

The entire flow field is viscous here, and is given mainly by the linear interactions between the oscillatory pressure gradient and the viscous term in the w equation, and between the centrifugal force and the viscous term in the χ equation. For the circular tube, therefore,

$$w_{00} = (\tfrac{1}{2}R_s)^{\frac{1}{2}}(1-r^2)\cos\tau, \quad \chi_{00} = \tfrac{1}{144}R_s r(1-r^2)^2(1-\tfrac{1}{4}r^2)\sin\psi\cos^2\tau. \tag{3.15}$$

Higher-order approximations are also readily calculable, as are the solutions for flow within rectangular or triangular tubes. The disturbances w_1 and χ_1 of (3.1) can then be expressed in similar fashion as

$$w_1 = w_{10} + O(\beta^{-3}), \quad \chi_1 = \beta^{-3}\chi_{10} + O(\beta^{-5}) \tag{3.16}$$

and we derive the solutions for the circle to be

$$w_{10} = \tfrac{1}{4}(1-r^2), \quad \chi_{10} = \tfrac{1}{288}(2R_s)^{\frac{1}{2}} r(r^2-1)(\tfrac{1}{4}r^2-1)\sin\psi\cos^2\tau. \tag{3.17}$$

Lastly in this section we emphasize that whilst the boundary-layer form of case I applied for large values of D (and of R_s), case II gives essentially a description of the flow pattern for small values of D, whatever the values of β and R_s. Moreover, in the steady limit I the centrifugal force drives the secondary streaming in both the core and the wall jet and the centrifuging is outwards in the core, whereas in the oscillatory limit the core centrifuging is partly inwards and there is practically no centrifugal effect except in the Stokes layer at high frequencies. Another strong contrast is that in case I (for $D \gg 1$) the secondary streamlines emanate from the boundary layer, which serves to determine the core motion, while in case II (for $\beta \ll 1$) there is no such outflow and the core motion consists of

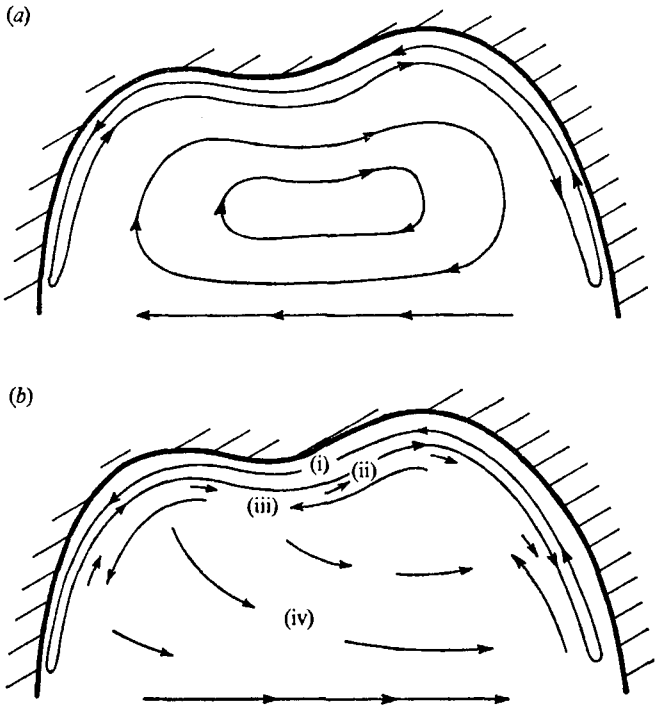

FIGURE 6. Sketches of the secondary streamlines in case III ($\beta \ll 1$) when (*a*) $D \ll 1$ (cf. Lyne 1971) and (*b*) $D \gg 1$. In (*b*), (i) is the Stokes layer, (ii) the steady slip layer, (iii) the steady boundary layer and (iv) is the steady interior of the core. Only the upper half of the arbitrary section is shown.

two vortices rotating in opposite directions (see figure 6). In consequence the transition between the two is not a straightforward matter (except via the full equations of motion (1.4) and (1.5) and we shall now discuss some further limiting situations and show how the two fundamental limits, cases I and II, may be joined through a succession of asymptotic descriptions. Case II in fact switches to the following case III for β and D both small, and to case VIII below for $\beta \gg 1$ and $D \ll 1$, when R_s is of order unity.

4. Case III: $\beta \ll 1$, $D, R_s \sim 1$

This high frequency limit is significant because, among other things, it shows how the secondary streaming, while remaining steady, alters from the patterns given by Lyne (1971) (see § 3) to those of the Dean equations (2.3) by way of crucially modified Dean equations. When β is small it transpires that in the core the time variation of w must be balanced by the dominant, oscillating, part of the pressure gradient, and yet the steady pressure gradient induces a disturbance in the down-pipe velocity whose centrifuging drives the secondary streaming. Thus

$$w = \beta^{-1}w_0 + w_1 + O(\beta), \quad \chi = \chi_0 + \beta\chi_1 + O(\beta^2), \tag{4.1}$$

where w_1, χ_0 and χ_1 are independent of τ but

$$w_0 = (2R_s)^{\frac{1}{2}} \sin\tau. \tag{4.2}$$

This leaves, from the governing equations (1.4) and (1.5), the equations

$$\left.\begin{aligned} -\partial(\chi_0, \nabla^2\chi_0)/\partial(x,z) - 2w_1\,\partial w_1/\partial z &= \nabla^4\chi_0, \\ -\partial(\chi_0, w_1)/\partial(x,z) &= D + \nabla^2 w_1 \end{aligned}\right\} \tag{4.3}$$

to determine w_1 and χ_0, with the boundary conditions

$$\chi_0 = w_1 = 0 \quad \text{at the wall} \tag{4.4}$$

along with (4.5) below.

Then in the Stokes layer, where $\eta = \beta^{-1}n \sim 1$ for the arbitrary cross-section,

$$w = \beta^{-1}W_0 + O(1), \quad \chi = \beta X_0 + O(\beta^2).$$

W_0 and X_0 are seen to be Lyne's extended solutions, laid down in (3.9), which comply with the no-slip conditions at $\eta = 0$. Since, therefore, $X_0 \sim -\frac{1}{4}\eta R_s\mu(x)$ as $\eta \to \infty$ we require the third boundary condition on (4.3) to be

$$\partial\chi_0/\partial n = -\tfrac{1}{4}R_s\mu(x) \quad \text{at the wall.} \tag{4.5}$$

Hence despite the dominance of the oscillating velocity (4.2) the steady secondary streaming χ_0 and secondary down-pipe velocity w_1 are controlled, interestingly enough, by Dean's steady equations (4.3) but with the novel boundary conditions (4.4) and (4.5), which are interpreted physically as a slip velocity along the tube wall and arise from the action of the unsteady centrifugal force, which is confined to the Stokes layer. We shall content ourselves here with the following asymptotic solutions proposed for small and large values of the Dean number D (§ 4.1) and of the secondary Reynolds number R_s (§ 4.2).

4.1. $D \ll 1$ *or* $D \gg 1$, $R_s \sim 1$

If D is first taken to be small the match with case II in § 3.1 is achieved, since

$$\chi_0 = \chi_{00} + D\chi_{01} + O(D^2), \quad w_1 = Dw_{10} + D^2 w_{11} + O(D^3). \tag{4.6}$$

In (4.3) this leaves χ_{00} governed by the high frequency equation (3.3), implying *inward* 'centrifuging' along the centre-line (see figure 6 and Lyne 1971), while w_{10} obeys (3.6) again. As in § 3.1, results for $R_s \ll 1$ and $R_s \gg 1$ are then derivable because χ_{00} is known explicitly.

For large values of D, however, with $R_s \sim 1$ the core flow (4.3)–(4.5) itself splits up into a double-layered structure. Within the interior of the core, it is found that

$$\chi_0 = D^{\frac{1}{3}}\chi_0^{(0)} + \chi_0^{(1)} + O(D^{-\frac{1}{3}}), \quad w_1 = D^{\frac{2}{3}}w_1^{(0)} + D^{\frac{1}{3}}w_1^{(1)} + O(1), \tag{4.7}$$

the orders of magnitude being apparent from the arguments of § 2.2. Thence and from (4.3), the core flow is characterized by

$$w_1^{(0)} = w_1^{(0)}(x), \quad \chi_0^{(0)} = z/w_1^{(0)\prime}(x), \tag{4.8}$$

where $w_1^{(0)}(x)$ must be calculated in the boundary layer, in which $n \sim D^{-\frac{1}{3}}$ and the asymptotic expansions for w_1 and χ_0 are effectively those for w_0 and χ_0 in (2.12). Following the analysis through shows that $D^{-\frac{2}{3}}w_1$ and $D^{-\frac{1}{3}}\chi_0$ are exactly the steady solutions W_0 and X_0 of the high Dean number equations (2.13) and (2.14), as the slip velocity in (4.5) is negligible when $D \gg 1$, and thus *outward*

centrifuging is promoted. A thinner slip region of thickness $O(D^{-\frac{2}{3}})$ is in fact needed to accommodate the slip velocity but that is of secondary importance. As figure 6 shows in this situation, at any station across the tube there are four distinct regions of flow and the steady streaming exhibits remarkable changes in direction. It is inward very close to the wall, in the Stokes layer, outward at the edge of the Stokes layer and in the above-mentioned sublayer, changes to a strong inward jet motion again in the steady boundary layer and finally becomes a relatively slow outward drift in the main core.

4.2. $D \sim 1$, $R_s \ll 1$ *or* $R_s \gg 1$

When R_s is small the basic problem (4.3)–(4.5) reverts to the conventional Dean problem (2.3) and (2.4) for order-one values of D because the slip velocity in (4.5) is then a secondary influence. So w_1 and χ_0 are expressible as

$$w_1 = w_{10} + R_s w_{11} + O(R_s^2), \quad \chi_0 = \chi_{00} + R_s \chi_{01} + O(R_s^2), \tag{4.9}$$

where w_{10} and χ_{00} satisfy (2.3) and (2.4), and only in the perturbation χ_{01} does the effect of the wall slip become evident.

In contrast, when R_s is large and $D \sim 1$ it is chiefly the influence of the slip velocity generated by the Stokes layer that drives the core motion, and the flow features are of a quite different character. Now χ_0 is governed principally by the large-R_s motion given by the Navier–Stokes equation (3.3), due to Lyne (1971), wherein the vorticity is $-\zeta R_s$ and ζ is a constant (equal to 0·56 for the circle) throughout most of the core. The initial expectation was that w_1 would be controlled by the steady pressure distribution in (4.3) for the most part, but after this work was completed the author learned the details of Blennerhassett's (1976) concurrent but more comprehensive investigation of the present limit (for $D \ll 1$), which does seem to be one of the most interesting features of our pulsatile flow studies. His numerical solutions, substantiated analytically, show the surprising result that D does not enter the main balance of forces at all. For the full details we therefore refer to his work (which is concerned more with a precise detailed examination of the possible flow fields rather than with the broader aspects that are the concern of this paper).

The large-D limit in § 4.1 does not match directly with that in case I, because the velocity along the pipe is still effectively given by (4.2). Rather, it leads to case IV below; for, as the Dean number is increased the chief assumptions of case III are invalidated when D reaches the order of $\beta^{-\frac{3}{2}}$ [since then $\beta^{-1} w_0 \sim w_1$ in (4.1)], and this defines the essential property of case IV, studied next. Physically, in case III, the strong oscillatory down-pipe velocity, produced by the mainly oscillatory pressure gradient, itself induces a negligible centrifugal force in the core, which is why the relatively weak steady gradient is able to interact with the inertial force of the secondary motion there and allows a trend towards outward secondary flow. However the centrifugal effect of the oscillatory component becomes appreciable in the thin Stokes wall layer, where the flow is dominated by the unsteadiness, and so the effective slip velocity, with its tendency to provoke some inward secondary core motion, is also promoted.

5. Case IV: $D \gg 1, \beta \sim D^{-\frac{2}{3}}, R_s \sim 1$

The important points about this new limit of the governing equations are that it generates a relatively simple *pulsating* down-pipe velocity, with steady secondary velocities, and also that the merging of cases III above and V below is achieved. Moreover, the pulsatile solution can be found explicitly. Both the high frequency results in § 3.1 and the high Dean number studies of § 2.2 propose the same order of magnitude, $D^{\frac{2}{3}}$, for w in the inviscid core. The steady flows, however, suggest that χ is $O(D^{\frac{1}{3}})$ and a viscous boundary layer of thickness $\sim D^{-\frac{1}{3}}$, in contrast to the oscillatory flows, where χ is $O(1)$ in the core and the viscous Stokes layer has thickness $\sim \beta = \tilde{k}D^{-\frac{2}{3}}$, say, wherein $\chi \sim \beta$. (Here $\tilde{k}$ is an order-one constant.) Accordingly we find that the motion must be examined in three distinct but inter-related stages, the three-tiered structure being in line with the findings of § 4.1. First, in the core

$$w = D^{\frac{2}{3}}w_0 + D^{\frac{1}{3}}w_1 + \ldots, \quad \chi = D^{\frac{1}{3}}\chi_0 + \chi_1 + \ldots \tag{5.1}$$

reduces the governing equations from (1.4) and (1.5) to the separate forms

$$\frac{2}{\tilde{k}^2}\frac{\partial}{\partial\tau}(\nabla^2\chi_0) = 0, \quad \frac{2}{\tilde{k}^2}\frac{\partial}{\partial\tau}(\nabla^2\chi_1) = 2w_0\frac{\partial w_0}{\partial z}, \quad \frac{2}{\tilde{k}^2}\frac{\partial}{\partial\tau}(\nabla^2\chi_2) = 2\frac{\partial}{\partial z}(w_0w_1), \tag{5.2a}$$

$$\frac{2}{\tilde{k}^2}\frac{\partial w_0}{\partial\tau} = \frac{2}{\tilde{k}^3}(2R_s)^{\frac{1}{2}}\cos\tau, \quad \frac{\partial w_1}{\partial\tau} = \frac{\partial w_2}{\partial\tau} = 0, \quad \frac{2}{\tilde{k}^2}\frac{\partial w_3}{\partial\tau} - \frac{\partial(\chi_0, w_0)}{\partial(x,z)} = 1 \tag{5.2b}$$

and so on. So $w_0 = \tilde{k}^{-1}(2R_s)^{\frac{1}{2}}\sin\tau + f_0(x,z)$, where f_0 is an unknown function of x and z, and w_1 and w_2 are steady. Modifying Lyne's (1971) reasoning for the present example, $\chi_0 = \chi_0(x,z)$ must also be steady, implying the same for $w_3(x,z)$ from (5.2b). Postulating that $f_0(x,z)$ is not identically zero then yields, from the steady component of the second equation in (5.2a), that f_0 is independent of z, and accordingly w_0 and χ_0 are fixed by

$$w_0 = \tilde{k}^{-1}(2R_s)^{\frac{1}{2}}\sin\tau + f_0(x), \quad \chi_0 = z/f_0'(x) \tag{5.3}$$

and the down-pipe velocity is pulsatile, with its steady component $f_0(x)$ to be determined.

Within the $D^{-\frac{1}{3}}$ boundary layer, where $N = D^{\frac{1}{3}}n$ and s are the relevant co-ordinates,

$$w = D^{\frac{2}{3}}W_0 + D^{\frac{1}{3}}W_1 + \ldots, \quad \chi = D^{\frac{1}{3}}X_0 + X_1 + \ldots . \tag{5.4}$$

Then the successive balances in (1.4) and (1.5) are

$$\left.\begin{aligned} &\frac{\partial}{\partial\tau}\left(\frac{\partial^2X_0}{\partial N^2}\right) = \frac{\partial}{\partial\tau}\left(\frac{\partial^2X_1}{\partial N^2}\right) = 0, \\ &\frac{2}{\tilde{k}^2}\frac{\partial}{\partial\tau}\left(\frac{\partial^2X_2}{\partial N^2}\right) - \frac{\partial(X_0, \partial^2X_0/\partial N^2)}{\partial(s,N)} + 2W_0\frac{\partial W_0}{\partial N}\mu(x) = \frac{\partial^4X_0}{\partial N^4} \end{aligned}\right\} \tag{5.5a}$$

and

$$\left.\begin{aligned} &\frac{2}{\tilde{k}^2}\frac{\partial W_0}{\partial\tau} = \frac{2}{\tilde{k}^3}(2R_s)^{\frac{1}{2}}\cos\tau, \quad \frac{\partial W_1}{\partial\tau} = 0, \\ &\frac{2}{\tilde{k}^2}\frac{\partial W_2}{\partial\tau} - \frac{\partial(X_0, W_0)}{\partial(s,N)} = \frac{\partial^2W_0}{\partial N^2}. \end{aligned}\right\} \tag{5.5b}$$

Therefore the unsteady and steady components can be uncoupled in the solution, leaving

$$W_0 = \tilde{k}^{-1}(2R_s)^{\frac{1}{2}} \sin\tau + \overline{W}_0(s,N), \quad X_0 = X_0(s,N), \tag{5.6}$$

where $\overline{W}_0(s,\infty) = f_0(x)$ and both W_1 and W_2 are steady, as is X_1. The term X_2 however is time dependent and is given, from (5.5) and (5.6), by

$$X_2(s,N,\tau) = \tilde{k}(2R_s)^{\frac{1}{2}} \cos\tau \left\{ \int_0^N \overline{W}_0(s,N_1)\, dN_1 + A(s,\tau)\, N + B(s,\tau) \right\} \mu(x) + \overline{X}_2(s,N), \tag{5.7}$$

with $A(s,\tau)$, $B(s,\tau)$ and $\overline{X}_2(s,N)$ to be determined. The boundary conditions we stipulate for X_2 are $X_2(s,0,\tau) = 0$, for zero normal velocity at the pipe wall $N = 0$, and, most important, that X_2 must be finite when N tends to infinity, to avoid a contradiction in solving for χ_1 in (5.2*a*). So

$$B(s,\tau) = 0, \quad A(s,\tau) = -f_0(x),$$

and in the core the unsteady part $\chi_2^{(u)}$ of χ_2 then satisfies Laplace's equation $\nabla^2\chi_2^{(u)} = 0$, subject to

$$\chi_2^{(u)} = \tilde{k}(2R_s)^{\frac{1}{2}} \cos\tau \int_0^\infty [\overline{W}_0(s,N_1) - f_0(x)]\, dN_1 \mu(x)$$

on the surface $n = 0$. A slip velocity now persists in the boundary layer along $N = 0$ and is given by $\partial X_2(s,0,\tau)/\partial N$ in (5.7), which is non-zero in general. Also (5.5) now show that $\overline{W}_0$ and X_0 are simply the known steady boundary-layer solutions of § 2.2, and $f_0(x)$ is thereby determined.

The steady component of W thus tends to zero at the pipe wall $N = 0$ but the oscillatory part remains as it was in the core. To reduce the latter to zero the viscous Stokes ($D^{-\frac{3}{4}}$) layer, buried within the steady viscous layer, comes into operation. There $\eta = \tilde{k}^{-1} n D^{\frac{3}{4}}$ is of order unity and

$$w = \tilde{k}^{-1} D^{\frac{3}{4}} \hat{W}_0 + \ldots, \quad \chi = \tfrac{1}{2}\tilde{k}^2 D^{-\frac{1}{2}} \tau_0(x)\, \eta^2 + \tilde{k} D^{-\frac{3}{4}} \hat{X}_1 + \ldots, \tag{5.8}$$

the major shearing term $\tau_0(X)$ in χ being forced by the (known) steady skin friction due to (5.6). Substitution into the equations of motion (1.4) and (1.5) reveals $\hat{W}_0$ to be the solution βw_0 in (3.9*a*), since $\hat{W}_0 \to (2R_s)^{\frac{1}{2}} \sin\tau$ as $\eta \to \infty$; however, $\hat{X}_1$ differs from (3.9*b*) because its growth as $\eta \to \infty$ must not only fit the linear behaviour of (5.7) for $N \ll 1$ but also the parabolic behaviour as $N \to 0$ of the steady term $X_1 \sim \frac{1}{2}\tau_1(x)\, N^2$, say. Such an argument requires that

$$\hat{X}_1 = \tfrac{1}{2}\tau_1(x)\, \tilde{k}\eta^2 + \tilde{k} R_s^{\frac{1}{2}} \mu(x) f_0(x) \left[\cos(\tau - \tfrac{1}{4}\pi) - e^{-\eta}\cos(\tau - \eta - \tfrac{1}{4}\pi) - 2^{\frac{1}{2}}\eta\cos\tau\right] + R_s\mu(x)\{-\tfrac{1}{4}\eta + O(1)\}, \tag{5.9}$$

where the term in curly brackets is the same as that given in (3.9*b*) above. Solution (5.9) satisfies no slip at $\eta = 0$ and as $\eta \to \infty$ merges with the steady boundary layer, but it also imposes on $\overline{X}_2$ in (5.7) the slip conditions $\overline{X}_2 = 0$ and $\partial\overline{X}_2/\partial N = -\frac{1}{4}R_s\mu(x)$ at $N = 0$.

The fundamental nature of the pulsatile solution has therefore been completely determined for case IV. One may indeed continue to lower-order terms in the three zones but the interplay between the inviscid core and the steady and unsteady viscous layers becomes increasingly complicated, although in principle

any number of terms could be deduced. Further, when $\tilde{k} \to 0$ the flow clearly switches precisely into case III (§4.1) for $O(1)$ values of R_s, as the sinusoidal behaviour of w_0 in (5.3) becomes dominant. At the other extreme, when $\tilde{k} \to \infty$ with $R_s \sim 1$ and the steady term in (5.3) overrides the oscillatory one, the flow in essence reduces to a completely steady motion and the solutions join with case V below. Finally, for $\tilde{k}$ and R_s both large a continuation into case X (see § 8) is achieved. Case IV therefore acts as a junction between flows for $R_s \sim 1$ and those for which $K \propto D^{\frac{3}{2}}$, studied in §§ 7 and 8 below.

Here in case IV there are again pronounced changes in the direction of the streaming and figure 6(*b*) in fact still gives an adequate representation of this secondary flow. Further, the pulsatile motion (5.3) is produced despite the smallness of the steady component of the pressure gradient in relation to the unsteady one, because the frequency of the unsteady component, though large, is not large enough to override the strength of the steady flow, which is largely responsible for the outward secondary streaming.

6. The other significant limits for $R_s \sim 1$ (cases V–VIII)

6.1. *Case* V: $D \gg 1$, $\beta \sim D^{-\frac{1}{3}}$, $R_s \sim 1$

If $\beta = \tilde{l} D^{-\frac{1}{3}}$ with $\tilde{l} \sim 1$, $D \gg 1$ and $R_s \sim 1$, then the steady and unsteady theories of §§ 2 and 3 both indicate the presence of an inviscid core and of viscous layers of thickness $\sim D^{-\frac{1}{3}}$ adjoining the wall. Again, the imposed pressure-variation terms in (1.5) are of *equal* orders of magnitude (D). So it is somewhat surprising to discover that the motion here is largely a steady one, developing in the core exactly as in (5.1), where now $w_0 = w_0(x)$ and $\chi_0 = z[w_0'(x)]^{-1}$ are the main components. The reason is simply that the oscillations in the pressure variation are too slow to affect the large steady down-pipe motion. The oscillating part of the pressure gradient merely promotes the secondary down-pipe motion and streaming,

$$w_1 = \tilde{l}^{-1}(2R_s)^{\frac{1}{2}} \sin\tau + f_1(x), \quad \chi_1 = \frac{z}{w_0'}\left\{w_0'' - \frac{f_1'}{w_0'}\right\} \tag{6.1}$$

respectively, and the lower-order contributions $w_2, w_3, \ldots$, are steady, as is χ_1.

In the $D^{-\frac{1}{3}}$ boundary layer, in similar fashion, w and χ behave to first order as in case I for large values of D, so that if $n = D^{-\frac{1}{3}}N$

$$\left.\begin{aligned} w &= D^{\frac{2}{3}}W_0(s,N) + D^{\frac{1}{3}}W_1(s,N,\tau) + \ldots, \\ \chi &= D^{\frac{1}{3}}X_0(s,N) + X_1(s,N,\tau) + \ldots. \end{aligned}\right\} \tag{6.2}$$

Here W_0 and X_0 are the steady large-D solutions (§ 2.2) and the unsteady perturbations W_1 and X_1 are fixed by the nonlinear equations

$$\left.\begin{aligned} \frac{2}{\tilde{l}^2}\frac{\partial}{\partial\tau}\left(\frac{\partial^2 X_1}{\partial N^2}\right) - \frac{\partial(X_0, X_{1NN})}{\partial(s,N)} - \frac{\partial(X_1, X_{0NN})}{\partial(s,N)} + 2\frac{\partial}{\partial N}(W_1 W_0)\mu(x) &= \frac{\partial^4 X_1}{\partial N^4}, \\ \frac{2}{\tilde{l}^2}\frac{\partial W_1}{\partial\tau} - \frac{\partial(X_0, W_1)}{\partial(s,N)} - \frac{\partial(X_1, W_0)}{\partial(s,N)} &= 1 + \frac{2}{\tilde{l}^3}(2R_s)^{\frac{1}{2}}\cos\tau + \frac{\partial^2 W_1}{\partial N^2}, \end{aligned}\right\} \tag{6.3}$$

subject to no-slip conditions at $N = 0$ and

$$W_1 \to \frac{(2R_s)^{\frac{1}{2}}}{\tilde{l}} \sin\tau + f_1(x), \quad X_1 \to \frac{-N}{\mu(x) w_0'} + \frac{g(x)}{w_0'} \left\{ w_0'' - \frac{f_1'}{w_0'} \right\} \tag{6.3a}$$

as $N \to \infty$. One outstanding aspect of (6.3) is the way all the forces possible in the current pipe-flow model are combining to control the disturbance velocities. (A similar feature arises for the basic flow field of case X below.) Equations (6.3) and (6.3*a*) should be sufficient to enable $f_1(x)$ to be ascertained. A linearized form of solution similar to that employed by Weyl (1941) for the boundary-layer equations adds weight to this argument, but we observe that despite the basically steady properties of this motion the unsteady disturbances are of quite different character from those in the classic limit of § 2.2. Hence case V does not match immediately with case I. It does with case IV when $\tilde{l}$ is small and R_s is $O(1)$; the nonlinear $D^{-\frac{1}{3}}$ boundary layer (6.3) itself then sub-divides into two parts, a steady region when $N \sim 1$ and an inner (Stokes) layer appearing when $N \sim \tilde{l}$, and their relation is along the lines of the discussion in § 5. Further, case V connects with case *X* below if R_s is taken to be suitably large.

For values of R_s of order one, this completes the description of the solution when one of the numbers β and D is small (i.e. cases II–V) and we shall now discuss the remaining possibilities, not so far covered, occurring when either β or D is large. Plainly cases I, IV and V provide some inroads into this regime but to join cases I and V, as β decreases, and case I to case II, as both D and β decrease, seems to require the introduction of some 'buffer' cases, namely cases VI–VIII, which we shall now describe briefly. Two of these new limits are of an essentially steady nature and match with case I in appropriate conditions but the third, case VIII, is another pulsatile motion.

6.2. *Cases* VI–VIII: $R_s \sim 1$, D *or* $\beta \gg 1$

When $D \gg 1$ and $\beta \sim 1$ (case VI) the flow field has the familiar form (5.1) in the core and (6.2) in the $D^{-\frac{1}{3}}$ boundary layer, motivated by cases I and V above. Both (w_0, χ_0) and (W_0, X_0) are the known steady solutions for large values of the Dean number and only in the perturbations do differences from case I appear. For the sake of brevity we shall not go into the precise details of case VI here, as the expansions and resulting equations are straightforward but rather lengthy and in effect the unsteadiness is so weak that no new pulsatile phenomena appear. It is found however that for $\beta \to 0$ the solution in case VI continues into case V, while for $\beta \to \infty$ it leads to case VII, defined by $\beta \gg 1$, $D \sim 1$ and $R_s \sim 1$. Here

$$w = w_0 + \beta^{-3}(2R_s)^{\frac{1}{2}} w_1 + \ldots, \quad \chi = \chi_0 + \beta^{-3}(2R_s)^{\frac{1}{2}} \chi_1 + \ldots . \tag{6.4}$$

Such expansions lead to the full Dean equations (2.3) and (2.4) for w_0 and χ_0 and evidently the disturbances w_1 and χ_1 are identical with those governed by (2.5), even though R_s is smaller here, so that the solution to (6.4) is assumed already and the match with case I is straightforward. As $D \to \infty$, case VII therefore exhibits the form (2.10) ff. and merges into the large-β limit of case VI. For small values of D, case VII gives the Poiseuille flow results (2.6) and (2.7) for w_0 and χ_0 and (2.8) and (2.9) for w_1 and χ_1. Consequently the structure of case VII strictly breaks

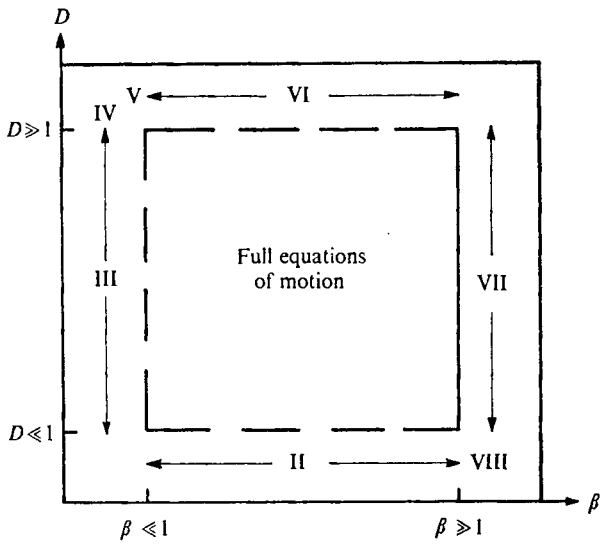

FIGURE 7. Schematic diagram showing the ranges of validity and interconnexions of cases II–VIII, asymptotic solutions for R_s of order unity. *Diagram not to scale.*

down, for small D values, when $\beta \sim D^{-\frac{1}{2}} \gg 1$ since then w_0 and $\beta^{-3}w_1$ in (6.4) shrink to the same order of magnitude, D.

Case VIII is therefore invoked to cope with the new situation $R_s \sim 1$, $D \ll 1$, $\beta \sim D^{\frac{1}{3}}$. Writing $\beta = \tilde{m}D^{-\frac{1}{3}}$, where $\tilde{m} \sim 1$, then gives

$$w = Dw_0 + D^2w_1 + \ldots, \quad \chi = D^2\chi_0 + D^3\chi_1 \ldots . \tag{6.5}$$

Substituting (6.5) into (1.4) and (1.5) we deduce that w_0 and χ_0 are governed by the unsteady Poiseuille flow equations, implying the essentially straight-pipe *pulsatile* velocity distribution

$$w_0 = \tfrac{1}{4}(1-r^2)\,[1 + (2/\tilde{m}^3)\,(2R_s)^{\frac{1}{2}} \cos\tau] \tag{6.6}$$

for a circular tube. Hence the secondary streaming is

$$\chi_0 = \frac{r(1-r^2)^2}{1152}\left(1-\frac{r^2}{4}\right)\left[1+\frac{2}{\tilde{m}^3}(2R_s)^{\frac{1}{2}}\cos\tau\right]^2 \sin\psi. \tag{6.7}$$

In conclusion, we have from (6.4)–(6.7) that case VIII merges with case VII as $\tilde{m} \to \infty$, as required, and furthermore, from (6.5)–(6.7) and § 3.2, case VIII reduces to the classic limit II for low frequencies, $\beta \gg 1$, as $\tilde{m} \to 0$. Cases II and VII can be seen almost to match directly but case VIII has been brought in anyway because it provides another illustration of an effectively pulsating core flow, equation (6.6). The asymptotic picture that we have built up of the pipe-flow features for order-unity values of R_s is thereby completed, and is summarized diagrammatically in figure 7.

Hereafter we focus on two limits of the governing equations that occur when R_s, as well as β, is allowed to depend on the Dean number D when D is large. The two limits selected (cases IX and X) produce a switch from the classic limit of steady flow, case I, to the only truly pulsating flow situation so far encountered

for $D \gg 1$, that of case IV, and we discover that in both instances the new distribution of down-pipe velocity is also pulsatile; but in case IX it is not of the relatively simple additive kind arising in case IV, and to a lesser extent in cases III and V, above. Such behaviour of the velocity field is naturally interesting in its own right. The common feature of the steady flow limit (2.1) and (2.2) and the pulsatile motion of case IV, (5.1)–(5.3), when $D \gg 1$ is the maintenance of the relationship $K \propto D^{\frac{2}{3}}$ in both, and so the next two situations investigated are both defined with this property preserved, the first situation occurring when $\beta \sim D^{-\frac{1}{6}}$ and the second when $\beta \sim D^{-\frac{1}{3}}$, for reasons set out in the following sections.

7. Case IX: $D \gg 1$, $R_s \sim D$, $\beta \sim D^{-\frac{1}{6}}$

Returning to the classic steady flow at high Dean number of § 2.2, we found there that the ratio of the major steady term in w to the unsteady disturbance was $D^{\frac{3}{2}}:(2R_s)^{\frac{1}{2}} D^{-\frac{1}{2}}\beta^{-3}$. Hence if K remains proportional to $D^{\frac{2}{3}}$, so that $R_s \propto \beta^2 D^{\frac{4}{3}}$, then these two contributions are of comparable orders of magnitude when $\beta \sim D^{-\frac{1}{6}}$, which imposes a restriction on the range of validity of case I and defines the first of the new limits that we now discuss. Let us set

$$\beta = \tilde{n} D^{-\frac{1}{6}}, \quad R_s = \tfrac{1}{2}\lambda^2 \tilde{n}^2 D \quad (D \gg 1), \tag{7.1}$$

where $\tilde{n}$ and λ are $O(1)$ and the expression for R_s is written in a manner that incorporates the relation $K = \lambda D^{\frac{2}{3}}$ of (2.30). The expansions in the core then follow immediately from § 2.2; thus

$$w = D^{\frac{2}{3}} w_0 + D^{\frac{1}{2}} w_1 + \ldots, \quad \chi = D^{\frac{1}{3}}\chi_0 + D^{\frac{1}{6}}\chi_1 + \ldots. \tag{7.2}$$

The centrifugal term remains the largest in the χ equation of motion (1.4), giving

$$w_0 = w_0(x, \tau), \tag{7.3}$$

while in the w equation (1.5) both time variation and inertia forces are balanced by the pressure gradient, which itself comprises both steady and oscillatory components. Hence, upon integration with respect to z and using symmetry, χ_0 takes the form

$$\chi_0 = z\left\{\frac{2}{\tilde{n}^2}\left[\lambda \cos\tau - \frac{\partial w_0}{\partial \tau}\right] + 1\right\} \Big/ \frac{\partial w_0}{\partial x}. \tag{7.4}$$

The viscous layer is positioned at $n = D^{-\frac{1}{3}} N$ and from (7.3) and (7.4)

$$w = D^{\frac{2}{3}} W_0(s, N, \tau) + D^{\frac{1}{2}} W_1(s, N, \tau) + \ldots, \quad \chi = D^{\frac{1}{3}} X_0(s, N, \tau) + D^{\frac{1}{6}} X_1(s, N, \tau) + \ldots. \tag{7.5}$$

This leads to the familiar boundary-layer equations

$$\left.\begin{aligned} -\frac{\partial(X_0, \partial X_0/\partial N)}{\partial(s, N)} + \{W_0^2 - w_0^2(x, \tau)\}\mu(x) &= \frac{\partial^3 X_0}{\partial N^3}, \\ -\partial(X_0, W_0)/\partial(s, N) &= \partial^2 W_0/\partial N^2, \end{aligned}\right\} \tag{7.6}$$

but now subject to the new constraints

$$\left.\begin{aligned} W_0 \to w_0(x, \tau), \quad \partial X_0/\partial N \to 0 \quad \text{as} \quad N \to \infty, \\ W_0 = X_0 = \partial X_0/\partial N = 0 \quad \text{at} \quad N = 0, \end{aligned}\right\} \tag{7.7}$$

where

$$X_0(s, \infty, \tau) = g(x)\left\{\frac{2}{\tilde{n}^2}\left[\lambda \cos\tau - \frac{\partial w_0}{\partial \tau}\right] + 1\right\} \Big/ \frac{\partial w_0}{\partial x} \tag{7.8}$$

serves to determine $w_0(x,\tau)$. Although no time derivative is involved in (7.5), the τ dependence of W_0, X_0, w_0 and χ_0 cannot in general be divorced from the steady parts. The problem posed by (7.6)–(7.8) seems to demand on the whole a numerical approach to the solution, which has not yet been attempted, but to demonstrate the proposed non-trivial nature of the pulsatility, i.e. that the down-pipe flow (7.3) is not simply a linear combination like (5.3), solutions may be generated for small and large values of $\tilde{n}$ respectively. As each solution includes series of terms in $\cos\tau$ and $\sin\tau$, it is reasonable to assert that the general behaviour of the core flow will be more subtle than in the previous pulsations explored in §§ 2–6.

For $\tilde{n} \gg 1$ the solutions may be expressed asymptotically as

$$\left.\begin{aligned} W_0(s,N,\tau) &= W_{00}(s,N) + \tilde{n}^{-2}W_{01}(s,N,\tau) + O(\tilde{n}^{-4}), \\ X_0(s,N,\tau) &= X_{00}(s,N) + \tilde{n}^{-2}X_{01}(s,N,\tau) + O(\tilde{n}^{-4}) \end{aligned}\right\} \tag{7.9}$$

and similarly for w_0 and χ_0. From (7.4)–(7.8) w_{00}, χ_{00}, W_{00} and X_{00} are then the steady solutions of the large-D equations in § 2.2, while $(2\lambda)^{-\frac{1}{2}}w_{01}$ and $(2\lambda)^{-\frac{1}{2}}\chi_{01}$ are identical with the disturbances $w_1^{(0)}$ and $\chi_1^{(0)}$ given in (2.21), and so on. This occurrence greatly enhances the importance of all the similarity flows in (2.25)–(2.29); for a pinched inside wall in particular, the pulsatile velocity down the pipe is

$$w_0 = Bx^{\frac{5}{6}} + \tilde{n}^{-2}Cx^{\frac{5}{6}}(2\lambda)^{\frac{1}{2}}\cos\tau + \tilde{n}^{-4}w_{02} + O(\tilde{n}^{-6}), \tag{7.10}$$

from (2.15) and (2.25), and subsequent examination based on the similarity variable η of (2.15) indicates that

$$w_{02} = C_2x^{\frac{5}{6}}\cos^2\tau + D_2x^{\frac{5}{3}}\sin\tau, \tag{7.11}$$

where C_2 and D_2 are constants to be determined from linear equations like (2.27). [Likewise the flow near the inner and outer walls of a circle follows from (2.28) and (2.29).] Thus case IX merges successfully with the large-D limit of case I. Conversely when $\tilde{n} \ll 1$ we believe that, whilst W_0, X_0 and χ_0 again develop according to (7.9) ff. (with $\tilde{n}^2$ replacing $\tilde{n}^{-2}$), w_0 is represented by

$$w_0 = [\lambda\sin\tau + f_{00}(x)] + \tilde{n}^2w_{01}(x,\tau) + O(\tilde{n}^4), \tag{7.12}$$

which reproduces the equations (7.6) for W_{00} and X_{00}, but with

$$W_{00} \to \lambda\sin\tau + f_{00}(x), \quad X_{00} \to \frac{g(x)}{f'_{00}}\left[1 - 2\frac{\partial w_{01}}{\partial\tau}\right] \tag{7.13}$$

as $N \to \infty$, because of (7.7) and (7.8). (This nonlinear problem may be solved in principle by extending Weyl's (1941) method and dealing with a series of linear equations, a procedure which can be expected to yield qualitatively correct information on the flow field here, as it does for the nonlinear flows in § 2.2, for instance.)

The complicated character of the pulsatility, strongly suggested by the solutions (7.9)–(7.13), and of the associated secondary velocities, is probably the point of foremost significance in case IX. In addition this has been the first example of a core/boundary-layer motion in which the secondary streaming is also largely unsteady, an occurrence connected with the actions of the pressure gradient, whose steady and unsteady parts are here of comparable magnitude.

When $\tilde{n}$ is large, for example, so that the motion is quasi-steady, the down-pipe flow pulsates nearly in plase with the pressure gradient, and while the secondary streaming remains outward (as in figure 6*b*) with its streamline directions largely unchanged, the strength of the secondary velocities also pulsates almost in phase. But when $\tilde{n}$ is small the pulsatility becomes $\frac{1}{2}\pi$ out of phase with the pressure gradient and the secondary streaming may exhibit reversals in direction during each time cycle, owing to the enhanced effect of the frequency of oscillation.

8. Case X: $D \gg 1, \beta \sim D^{-\frac{1}{3}}, R_s \sim D^{\frac{2}{3}}$

The results (7.12)–(7.14) show that, when $\tilde{n}$, defined in (7.1), becomes small and of order $D^{-\frac{1}{6}}$, the basic structure of case IX as set out in (7.2)–(7.5) fails owing to the gradual emergence of the other contributory forces. So we proceed to case X, with

$$\beta = \tilde{l}D^{-\frac{1}{3}}, \quad R_s = \tfrac{1}{2}\lambda^2\tilde{l}^2D^{\frac{2}{3}} \quad (D \gg 1). \tag{8.1}$$

Since now β is small and R_s and D are large, viscous effects are again confined to thin wall layers. More significantly, however, because β, $R_s^{-\frac{1}{2}}$ and $D^{-\frac{1}{3}}$ are comparable, Lyne's (1971) description of the oscillatory high frequency limit and its properties for $R_s \gg 1$, and Smith's (1975) study of the steady large-D range both lead to a $D^{-\frac{1}{3}}$ viscous layer, which may therefore be expected to depend on the interplay between inertial and centrifugal effects, unsteadiness and the oscillatory pressure variation, as well as viscous forces, and such proves to be the case in practice. Throughout the core, where expansions (7.2) again apply, the motion is mainly given by

$$\left.\begin{aligned} w_0 &= \lambda \sin\tau + f_0(x), \\ \chi_0 &= \left[z - \frac{2}{\tilde{l}^2}\int_0^z \frac{\partial w_1}{\partial \tau}\,dz\right]\Big/ f_0', \quad \frac{\partial}{\partial \tau}(\nabla^2\chi_0) = \tilde{l}^2 w_0 \frac{\partial w_1}{\partial z}. \end{aligned}\right\} \tag{8.2}$$

Even though the steady component of the pressure gradient is here much less than the unsteady one, they act together to induce the main, pulsatile, velocity w_0, while the steady gradient alone drives the secondary, unsteady, motion χ_0.

Near the walls of the tube the boundary layer and Stokes layer coincide, from the previous reasoning, and are placed where $N = D^{\frac{1}{3}}n \sim 1$. There the velocities are again expressible as in (7.5) and from (1.4) and (1.5) we derive the viscous equations

$$\left.\begin{aligned} \frac{2}{\tilde{l}^2}\frac{\partial}{\partial \tau}\left(\frac{\partial^2 X_0}{\partial N^2}\right) - \frac{\partial(X_0, \partial^2 X_0/\partial N^2)}{\partial(s, N)} + 2W_0\frac{\partial W_0}{\partial N}\mu(x) &= \frac{\partial^4 X_0}{\partial N^4}, \\ \frac{2}{\tilde{l}^2}\frac{\partial W_0}{\partial \tau} - \frac{\partial(X_0, W_0)}{\partial(s, N)} &= \frac{2\lambda}{\tilde{l}^2}\cos\tau + \frac{\partial^2 W_0}{\partial N^2}. \end{aligned}\right\} \tag{8.3}$$

The boundary conditions on (8.3) provide for no slip at $N = 0$ and for matching to the forms (8.2) at $z = g(x)$. The solution to (8.2) and (8.3) will be discussed for extreme values of the parameter $\tilde{l}$ (a small-λ analysis is also possible and leads to case V above), since a numerical treatment is again needed for the general situation.

When the value of $\tilde{l}$ is large a transition to the small-$\tilde{n}$ flow of case IX is anticipated, and it takes place in the form

$$W_0 = W_{00} + \tilde{l}^{-2}W_{01} + O(\tilde{l}^{-4}), \quad w_0 = [\lambda \sin\tau + f_{00}(x)] + \tilde{l}^{-2}w_{01}(x) + O(\tilde{l}^{-4}), \quad (8.4)$$

the expansions of χ_0 and X_0 also proceeding in powers of $\tilde{l}^{-2}$. The temporal variations in (8.3) are thereby suppressed, to first order in $\tilde{l}^{-2}$, and the problem (7.6) with (7.7) and its subsequent treatment along the lines of (7.12) ff. are retrieved. At the opposite extreme, $\tilde{l} \ll 1$, a partition of the boundary layer occurs, owing principally to the shrinking of the Stokes layer associated with the thickness $O(\tilde{l}D^{-\frac{1}{3}})$ instead of $O(D^{-\frac{1}{3}})$. The core-flow properties may be expressed in the manner of w_0 in (8.4), with $\tilde{l}^2$ replacing $\tilde{l}^{-2}$, and likewise W_0 develops as in (8.4) when N is of order one, except that now

$$W_{00} = \lambda \sin\tau + F_0(s, N), \quad (8.5)$$

where $F_0(s, N)$ and $X_{00}(s, N)$ are the classical steady boundary-layer solutions (§ 2.2). The steady contributions to the motion therefore satisfy the wall conditions at $N = 0$, but when N is small and $O(\tilde{l})$ the Stokes layer acts to deal with the $\lambda \sin\tau$ term in (8.5) and the τ-dependent forces in (8.3) are then recalled. This structure is basically that which arose in case IV, to which we refer for the precise details, and so the required junction with case IV, where $R_s \sim 1$, is effected.

Apart from the discovery of another pulsating motion along the tube, (8.2), and the coincidence of the Stokes (β), the steady ($D^{-\frac{1}{3}}$) and the secondary ($R_s^{-\frac{1}{2}}$) viscous layers in (8.3), the interest in case X lies in its completion of the development from case I to case IV for pipe flows in which (2.30) is preserved. The matching itself, I → IX → X → IV, is also intriguing as at both ends of the range the predominant secondary velocity is steady, whereas the intermediate limits IX and X possess the pulsatile characteristics (7.4) and (8.2). Further, the (linear) pulsatility in case X is produced by the presence of an applied steady pressure gradient much less in magnitude than the applied oscillatory part, whereas the (nonlinear) pulsations in case IX require equal orders of magnitude for the gradients. The persistence of the pulsatile nature from case IX to case X appears to be due to the associated increase in the frequency of the oscillatory component. The streaming in case X, as in case IX, may well be reversible when $\tilde{l}$ is large, but is definitely outward when $\tilde{l}$ becomes small because of the decrease in the secondary Reynolds number R_s.

9. Further discussion

Among the many aspects of the different flows produced by the imposed pulsatile pressure gradient (1.1) in a curved pipe, the (not unexpected) fact that the ratio $G/\rho^*\omega\overline{W}$ of the magnitude G of the steady component of the pressure variation to that of the unsteady component ($\rho^*\omega\overline{W}$) is not necessarily the primary feature determining the nature of the motion stands out perhaps the most. Table 1 presents the principal physical attributes of all the cases studied in this paper, along with the associated pressure-gradient ratios $G/\rho^*\omega\overline{W}$. Certainly in

Case	I	II	III	IV	V	VI	VII	VIII	IX	X
$G/\rho^*\omega\overline{W}$	$\gg 1$	$\ll 1$	$\ll 1$	$\ll 1$	$O(1)$	$\gg 1$	$\gg 1$	$O(1)$	$O(1)$	$\ll 1$
Down-pipe velocity	st.	osc.	osc.	puls.	st.	st.	st.	puls.	puls.	puls.
Secondary	st., O	st., I or O	st., I or O	st., O	st., O	st., O	st., O	puls., O	puls.	puls.

TABLE 1. The main characteristics of the down-pipe and secondary motions, and the pressure-gradient ratio $G/\rho^*\omega\overline{W}$, for cases I–X. Flows: st., steady; osc., oscillatory; puls., pulsating; I, inward; O, outward.

the three cases (I, VI and VII) where the steady amplitude is much greater than the amplitude of the oscillatory part, steady down-pipe flow is always produced, with the corresponding steady secondary streaming being outward. This seems to be due to the balancing of the steady pressure gradient by the down-pipe inertial and viscous forces, so that unsteadiness is not induced in the down-pipe flow, and this in turn leads to an interplay between the steady secondary inertial and viscous effects and the centrifugal force alone. However, if $G \ll \rho^*\omega\overline{W}$ (cases II–IV and X), so that the applied pressure variation is merely a small steady perturbation of the oscillatory variation, the flow may nevertheless be pulsatile because the frequency of the oscillations may not be high enough to overwhelm the influence of the steady gradient. This occurs in cases IV and X, where the oscillatory component has practically no effect on the inertial and centrifugal forces in the inviscid core and influences them only in the Stokes layer, thus allowing a steadily induced down-pipe velocity of magnitude comparable with the unsteady velocity in the core. In cases II and III, on the other hand, the oscillations are so fast that they do override the steady effect. Similarly in the three remaining cases (V, VIII and IX), where $G \sim \rho^*\omega\overline{W}$, although cases VIII and IX do produce pulsating down-pipe flows (the former a viscous inertia-free motion, the latter inviscid and inertial), the oscillations in case V are slow enough to permit the steady effect to dominate because again they have negligible inertial and centrifugal influence in the core. The need for the detailed analysis of each particular case therefore seems clear.

Since it is already known that both the fully steady and oscillatory motions can produce steady streaming (figure 6), one might be led to expect steady secondary flow for all pulsatile pressure gradients but this is not borne out in the detailed examinations. The first seven cases do exhibit steady streaming, whether inward or outward, but the straightforward viscous pulsatile–Poiseuille motion of case VIII and the much less obvious inviscid pulsatile core motions of cases IX and X all have associated pulsatility in the secondary velocities. In case IX the cause lies in the balance of all but the viscous forces in the down-pipe core flow, whereas in case X the secondary unsteadiness is forced by the presence of a small unsteady down-pipe velocity in addition to the main pulsatility.

For the flows with $R_s = O(1)$, cases II–VIII, in which nearly all the secondary motions are directed outward along the centre-line, presumably there exists a curve in the β, D parameter space of figure 7 marking the cross-over from fully outward to partly inward secondary streaming. The end points of this curve have

been shown to lie within the regimes of cases II and III, so that for $D \ll 1$ there is a finite value β_0 such that the secondary core flow is outward for $\beta > \beta_0$, while for $\beta \ll 1$ outward streaming is again promoted for $D > D_0$, where D_0 is a finite number to be determined. Apart from the need to make the general flow model more applicable to (for example) physiological situations, the determination of β_0 and D_0, in cases II and III, and numerical investigations of cases IX and X would appear to be the next most vital tasks to undertake, given the consistent picture of the transitions from one case to another presented in this work.

I am grateful to the referees for their helpful comments on this paper.

REFERENCES

BELCHER, R. J., BURGGRAF, O. R. & STEWARTSON, K. 1972 *J. Fluid Mech.* **52**, 753.

BLENNERHASSETT, P. 1976 In preparation.

CHENG, K. C. & AKIYAMA, M. 1970 *Int. J. Heat Mass Transfer*, **13**, 471.

DEAN, W. R. 1927 *Phil. Mag.* **4**, 208.

DEAN, W. R. 1928 *Phil. Mag.* **5**, 673.

ITO, H. 1969 *Z. angew. Math. Mech.* **49**, 653.

KUWAHARA, K. & IMAI, I. 1969 *Phys. Fluids Suppl.* **12**, II 94.

LYNE, W. H. 1971 *J. Fluid Mech.* **45**, 13.

MCCONALOGUE, D. J. & SRIVASTAVA, R. S. 1968 *Proc. Roy. Soc.* A **307**, 37.

SMITH, F. T. 1975 *Proc. Roy. Soc.* A (to appear).

STEWARTSON, K. 1957 *Proc. Symp. Boundary Layer Res., Int. Un. Theor. Appl. Mech., Freiburg*, p. 59.

WEYL, H. 1941 *Proc. Nat. Acad. Sci. Wash.* **27**, 578.